Experimental Evaluation of a Polycrystal Deformation Modeling Scheme Using Neutron Diffraction Measurements

BJØRN CLAUSEN and TORBEN LORENTZEN

The uniaxial behavior of aluminum polycrystals is simulated using a rate-independent incremental self-consistent elastic-plastic polycrystal deformation model, and the results are evaluated by neutron diffraction measurements. The elastic strains deduced from the model show good agreement with the experimental results for the 111 and 220 reflections, whereas the predicted elastic strain level for the 200 reflection is, in general, approximately 10 pct too low in the plastic regime.

I. INTRODUCTION

THE numerical simulations are based on an implementation[1] of a modeling scheme introduced by Hutchinson.[2] It is a rate-independent incremental self-consistent elastic-plastic model based on crystallographic slip in the grains. The model regards the polycrystal as an agglomerate of spherical single crystals, or grains, where the elastic and plastic interaction between the grains is taken into account by means of a self-consistent scheme. For further description of the model, refer to Reference 3. Polycrystal models are typically evaluated by their capability to simulate texture development. For large deformations and strong textures, model predictions are readily compared to textures determined experimentally, *i.e.*, by neutron diffraction, as shown in Reference 4. In the case of small deformations, however, the texture development is minimal and cannot serve as a means of evaluating the model predictions. However, the model can be evaluated on a much more specific micromechanical level using the novel technique of lattice strain characterization by neutron diffraction, as detailed in Reference 5. Neutron diffraction provides the possibility for an *in situ* determination of the elastic lattice strain in selected grain subsets within the polycrystal as a function of the applied load. Such results can be directly compared to model predictions of volume-average elastic lattice strains in selected grain subsets resembling the family of grains participating in the particular diffraction measurements.

II. THE POLYCRYSTAL MODEL

The initial critical resolved shear stress (τ_0) is identical on all the slip systems, and the rate of the critical resolved shear stress ($\dot{\tau}$) is determined by the hardening law. As described in Reference 3, the hardening law can be expressed as a relationship between the accumulated slip in the grains (γ^{acc}) and the instantaneous hardening coefficient (h_γ). The rate of the critical resolved shear stress is determined as

$$\dot{\tau}^i = \sum_j h^{ij}\dot{\gamma}^j \text{ where } h^{ij} = h_\gamma\,(q + (1 - q)\delta^{ij}) \qquad [1]$$

In the present implementation of this model, two different relations between h_γ and the accumulated slip in the grain are used: a linear function and an exponentially decreasing function. In the linear function, h_γ is given by a constant, h, times γ^{acc}. In the exponentially decreasing function, h_γ is described by the final hardening coefficient (h_{final}), the ratio between the initial and the final hardening coefficient (h_{ratio}), and a parameter that determines the strength of the exponential part (h_{exp}):

$$h_\gamma = h_{final}\,(1 + (h_{ratio} - 1)\,e^{(-h_{exp}\gamma^{acc})}) \qquad [2]$$

Selecting τ_0 and the hardening law, and, thus, the hardening coefficients, is not trivial. In this case, τ_0 and the hardening coefficients are determined by fitting the numerically predicted macroscopic stress-strain curve to experimental observations.

Using the linear hardening law, the simulated macroscopic stress-strain curve deviates from the experimental observations by showing a much sharper curvature at the onset of plasticity (Figure 1). The exponential decreasing hardening law, however, can be selected to make the numerical predictions match the experimental macroscopic stress-strain curve with an acceptable accuracy. The present calculations are based on the parameters listed in Table I, where it is to be noted that Taylor hardening ($q = 1$) is avoided as it causes the system of equations describing the slip rates to become an indeterminate system.

Even though the numerical model predictions of the macroscopic stress-strain curve can be made to match experimental observations, this does not provide verification of the model at a microstructural level, *i.e.*, whether stresses and strains in the grains are handled appropriately. An experimental evaluation at this level of detail is achievable, as the elastic lattice strains do lend themselves to experimental evaluation by diffraction techniques (*i.e.*, neutron diffraction), and we proceeded to such an experimental evaluation of the model predictions of elastic lattice strains in grain subsets within the polycrystal agglomerate.

III. EXPERIMENTAL

Neutron diffraction is widely used in materials science, where the main advantage is the penetration power of neu-

BJØRN CLAUSEN, Postdoc, formerly with the Materials Research Department, Risø National Laboratory, is with the Lujan Center, Los Alamos National Laboratory, Los Alamos, NM 87545. TORBEN LORENTZEN, Senior Scientist, is with the Materials Research Department, Risø National Laboratory, 4000 Roskilde, Denmark.

Manuscript submitted April 2, 1997.

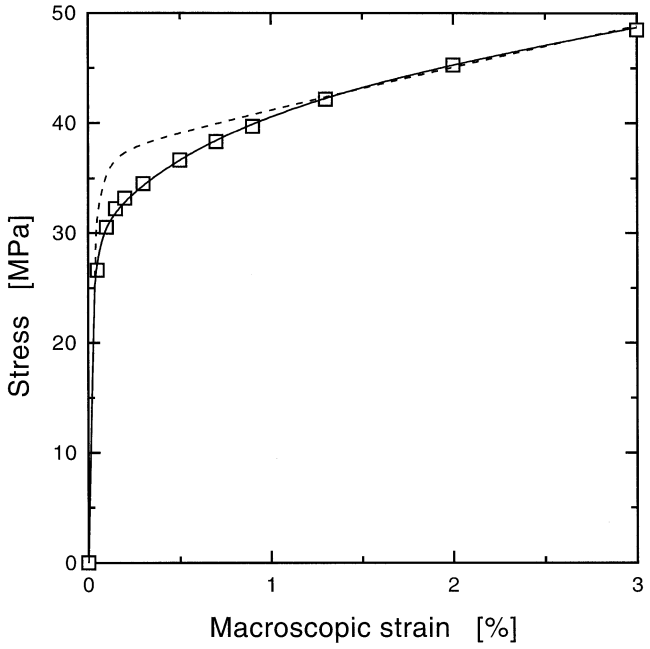

Fig. 1—Macroscopic stress-strain curves. (□) Experimental data. (—) Model calculation with exponentially decreasing hardening. (- - -) Model calculation with linear hardening.

trons, allowing bulk measurements centimeters into common metals like aluminum, copper, or iron. The neutron diffraction applications of primary interest in the present work are the determination of lattice strains and the determination of the initial sample texture.

A. *Lattice Strain Determination*

The neutron diffraction technique for lattice strain characterization in crystalline materials is based on Bragg's law, given by

$$\lambda = 2d_{hkl} \sin \theta \qquad [3]$$

where λ is the neutron wavelength, d_{hkl} is the lattice plane spacing of a selected *hkl* reflection, and θ is the diffraction angle. A variety of experimental configurations can be used; for examples, refer to References 5 and 7. The present experimental work is based on a single detector setup at the DR-3 steady-state research reactor at Risø National Laboratory. The experimental setup is shown in Figure 2, which indicates that a specific neutron wavelength is selected from the white beam of the reactor using a monochromator (M); in this case, a large single crystal of Germanium. Both incident and diffracted beams, which define the scattering vector (Q) are collimated (C), and the gage volume is defined by slit systems (S) made from a neutron-absorbing material, in this case, cadmium.

By scanning the single detector over an appropriate range of 2θ values, we determined the lattice plane spacing d_{hkl} of the specific grain subset, fulfilling the Bragg condition; this merely involves those crystallites having a specific lattice plane spacing, and their lattice plane normal aligned along the scattering vector. Lattice strains are determined by relating measured lattice plane spacings (d_{hkl}) to a stress-free reference value (d^0_{hkl}) following the relation

$$\varepsilon_{hkl} = \frac{d_{hkl} - d^0_{hkl}}{d^0_{hkl}} = \frac{\sin \theta^0}{\sin \theta} - 1 \qquad [4]$$

In the present work, samples are loaded in uniaxial tension using a stress rig developed for the spectrometer.[8] By aligning the tensile axis along the scattering vector, only the lattice strain along this axis is determined. The reference value (d^0_{hkl}) is here selected as the lattice plane spacing at zero load rather than a true stress-free value.

The number of grains fulfilling the Bragg condition depends on the gage volume size, the grain size, the texture, and the experimental resolution. As to the experimental resolution, only those grains oriented within ± 0.5 deg of the scattering vector will typically contribute to the measured intensity (Figure 2).

B. *Texture Characterization*

Texture characterization is also based on Bragg scattering, although the experimental setup differs from the one presented in Figure 2 (refer to Reference 4). By recording the intensity distribution of three *hkl* reflections over an appropriate part of Euler space, the orientation distribution function (ODF) is established. Based on this function, a representative set of grains is generated with the orientation of each grain given by the Euler angles, using the technique described in Reference 9. The present numerical calculations are made with such a set of 5796 grains, representing the experimentally determined initial texture of the material, which is commercially pure aluminum (AL2S) cold rolled and heat treated, rendering a grain size of approximately 100 μm. The ODF for the material used in the experiments shows that the material has a medium shear texture from the cold rolling during sample preparation (Figure 3).

IV. DISCUSSION

The hardening law in the model calculations is selected empirically to be of either a linear or an exponential form, and the parameters are adjusted to make the model prediction of the macroscopic stress-strain curve resemble the experimentally determined one. From the numerical results we extract the elastic strain component for specific *hkl* reflections, and these results form the basis of the model evaluation by comparison with the experimentally determined elastic lattice strain response. For this comparison only, the grain subsets fulfilling the Bragg condition should be considered. However, in a set of 5796 grains, as used in the present calculations, this would correspond to very few grains, and the deduced elastic strains would be prone to poor statistics. In practice, we selected the grains with the specific lattice plane normal within ± 5 deg of the tensile axis. The *in situ* neutron diffraction experiments were done in strain control, focusing on the 111, 200, and 220 reflections, while straining samples to a maximum of 3 pct macroscopic strain. For each reflection, two identical experiments were completed, and the results are presented as an average of these two.

In Figure 4, the evolution of measured elastic lattice strains is shown as a function of the macroscopic strain. The error bar represents the standard deviation of five con-

Table I. Aluminum Single-Crystal Stiffnesses[6] and Fitting Parameters for the Two Types of Hardening Laws

	C_{11} (GPa)	C_{12} (GPa)	C_{44} (GPa)	$\frac{2C_{44}}{C_{11} - C_{12}}$	τ_0 (MPa)	h_{final} (MPa)	h_{ratio}	h_{exp}	q
Linear	108.2	61.3	28.5	1.22	12.7	50.0	1.0	—	1.01
Exponential	108.2	61.3	28.5	1.22	10.9	40.0	5.0	61.0	1.01

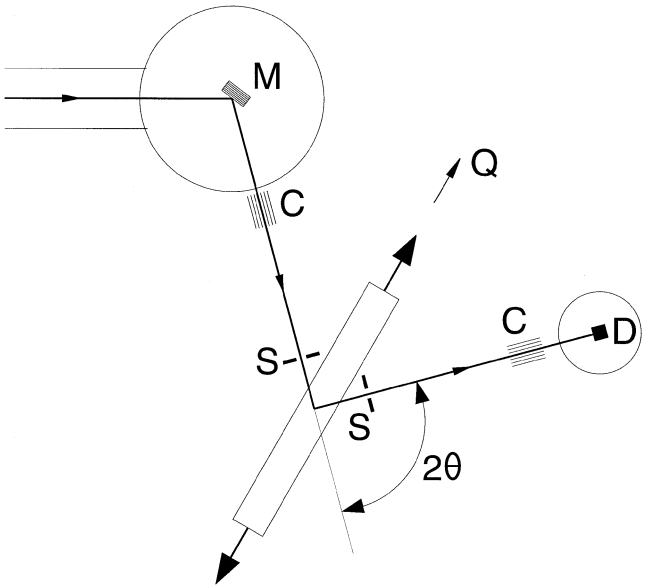

Fig. 2—Experimental setup at TAS8. C: collimator, D: detector, M: monochromator, Q: scattering vector, and S: slits.

secutive measurements. It is evident that the selected grain subsets display great differences, with the grain subset having the ⟨111⟩ lattice plane normal aligned along the tensile axis carrying the highest elastic strains, while the grain subset having the ⟨220⟩ lattice plane normal aligned along tensile axis carried the smallest elastic strains. Furthermore, it is observed that the general trend in all three curves resembles the macroscopic stress-strain curve, as shown in Figure 1.

The experimental results of Figure 4 are compared to the model predictions using either of the two selected hardening laws, and the results are presented in Figures 5 through 7. It is evident from these results that the exponential hardening law, which provides good agreement with the macroscopic stress-strain curve, also provides the closest agreement with experimental observations on a grain-size scale. For all three reflections, the experimental data show a smooth transition from the elastic region to the plastic region. None of the measurements follow the relatively sharp transition predicted when using the linear hardening law. The selected parameters for the calculation with the linear hardening law are a compromise between good agreement at the onset of yield or good agreement in the plastic regime, we have chosen the latter. Hence, it is concluded from the present data that the linear hardening law is a rather poor choice.

In comparing the model predictions of the individual lattice strain responses with the experimental observations, it is evident that the model predicts the elastic lattice strain evolution for the 111 and the 220 reflections quite accurately. For the 200 reflection, however, the discrepancy is

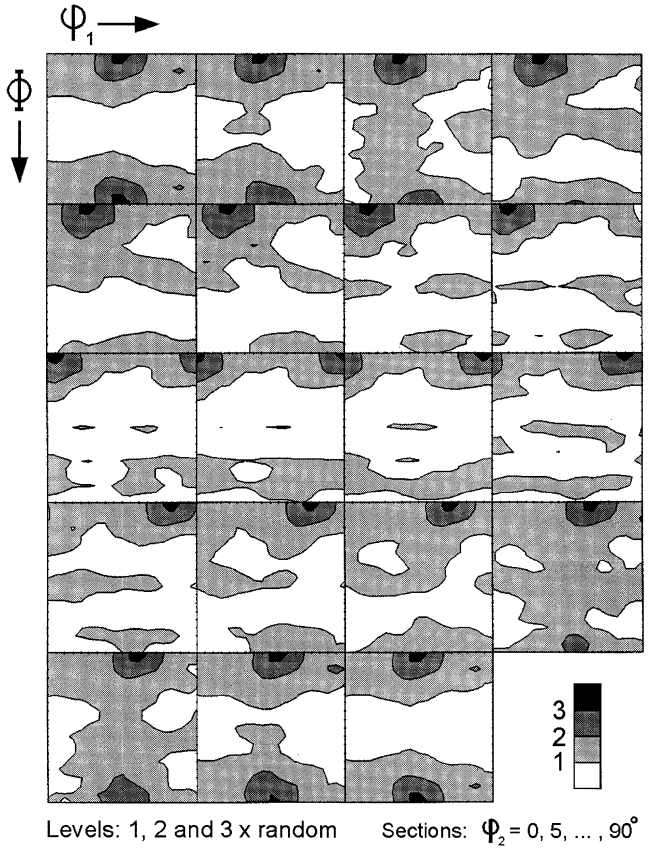

Fig. 3—ODF for the aluminum samples.

noticeable. For this reflection, all experimental results past the onset of yielding show higher elastic strains than predicted by the model, and at 1 pct total deformation, the model is underestimating the elastic strain level by approximately 10 pct. In comparing the results from all three grain subsets, it is furthermore noticed that the model predicts the 200 reflection to experience numerically lower elastic strains than the 220 reflection. This is in contradiction to the experimental observations. On the other hand, the model successfully predicts the numerical level of elastic strains in the 111 and 220 reflections.

V. CONCLUSIONS

In the present work, a well known self-consistent scheme for describing polycrystal deformation has been used to simulate uniaxial deformation of aluminum. We have selectively chosen to follow the evolution of elastic lattice strains in specific grain subsets, as such numerical results are directly comparable to actual experimental observations when using neutron diffraction. As such, the aim has been to evaluate the model predictions at a grain-size scale, rather than the usual evaluations based on tex-

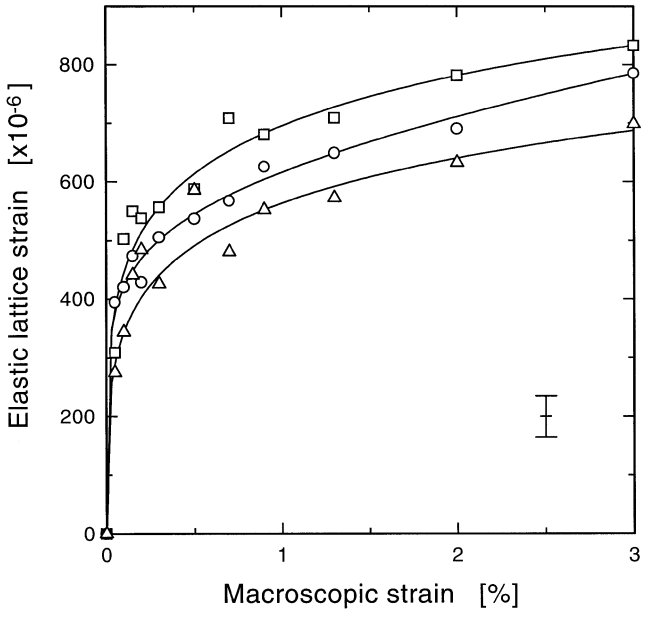

Fig. 4—Experimentally determined elastic lattice strain curves for the 111 reflection (□), the 200 reflection (○), and the 220 reflection (△). The lines are meant as ''guides to the eye.''

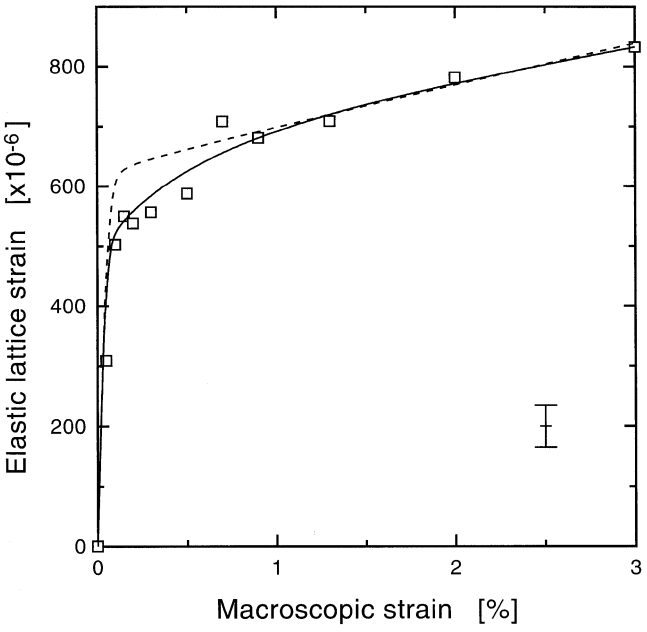

Fig. 5—Elastic lattice strain evolution for the 111 reflection. (□) Neutron diffraction. (—) Calculated with exponential hardening. (- - -) Calculated with linear hardening.

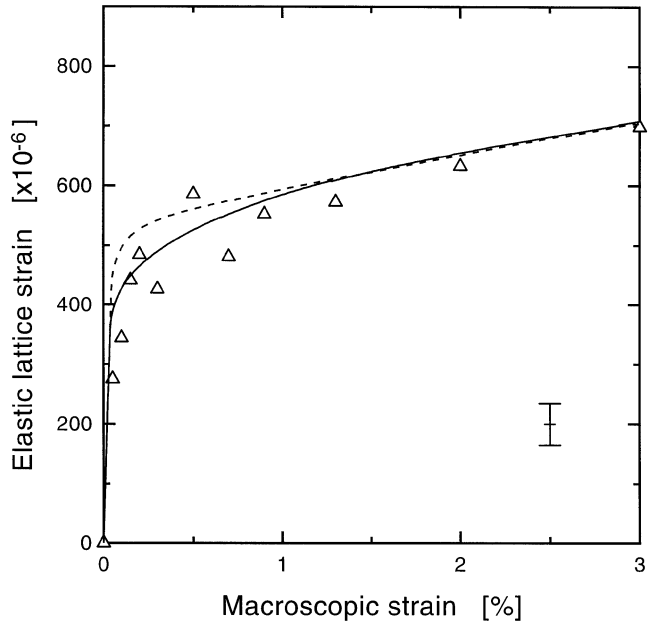

Fig. 6—Elastic lattice strain evolution for the 220 reflection. (△) Neutron diffraction. (—) Calculated with exponential hardening. (- - -) Calculated with linear hardening.

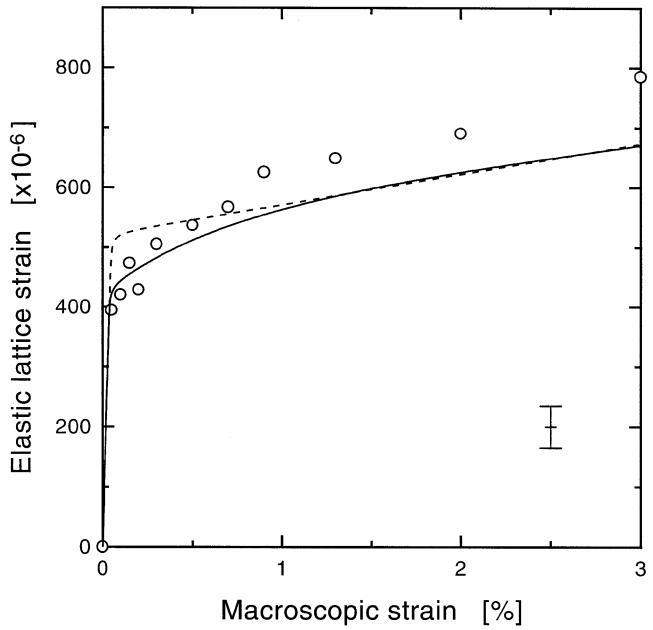

Fig. 7—Elastic lattice strain evolution for the 200 reflection. (○) Neutron diffraction. (—) Calculated with exponential hardening. (- - -) Calculated with linear hardening.

ture developments. The elastic lattice strain evolution was followed by diffraction in three grain subsets while straining the samples to 3 pct total strain. In comparison to the model predictions, it was found that calculations based on a linear hardening law do not successfully predict the onset of yielding. All the experimental results show a gradual transition from elasticity to plasticity that is more accurately predicted by the numerical results based on an exponential hardening law. These numerical predictions also show better agreement with actual experiments in terms of the overall macroscopic stress-strain response. The numerical predictions accurately reflect the elastic lattice strain evolution for the 111 reflection as well as for the 220 reflection.

For the 200 reflection, the model prediction agrees qualitatively with the experimental observations; however, with increasing macroscopic strain the model consistently underestimates the experimental observations. The discrepancy is, in general, merely on the order of 10 pct beyond a macroscopic strain of 1 pct; however, as the model consistently underestimates the lattice strain evolution for this *hkl* reflection, it is clear that the model is lacking some micromechanical mechanism explaining the relatively

''soft'' behavior of the 200 reflection. It may be argued that it is a too-crude assumption to select a hardening law which is identical for all orientations and slip systems. Specific hardening laws for particular orientations and slip systems can be readily introduced, although not without increasing the amount of empiric assumptions in the model. As a numerical exercise, the empiric selection of a range of hardening laws may be tested; however, we envisage that further experimental work using neutron diffraction may lead to a more qualified selection of more advanced hardening laws.

ACKNOWLEDGMENTS

The work was carried out within the Engineering Science Centre for Structural Characterisation and Modelling of Materials, Risø National Laboratory.

REFERENCES

1. B. Clausen and T. Lorentzen: *Risø-R-970(EN)*, Risø National Laboratory, Roskilde, Denmark, 1997.
2. J.W. Hutchinson: *Proc. R. Soc. London*, 1970, vol. A319, pp. 247-72.
3. B. Clausen: PhD Thesis, *Risø-R-985(EN)*, Risø National Laboratory, Roskilde, Denmark, 1997.
4. D. Juul Jensen and T. Leffers: *Textures Microstr.*, 1989, vol. 10, pp. 361-73.
5. A.J. Allen, M.T. Hutchings, C.G. Windsor, and C. Andreani: *Adv. Phys.*, 1985, vol. 34, pp. 445-73.
6. G.E. Dieter: *Mechanical Metallurgy*, 3rd ed., McGraw-Hill, New York, NY, 1988, p. 59.
7. T. Lorentzen: PhD Thesis, Aalborg University, Aalborg, Denmark, 1990.
8. T. Lorentzen and N.J. Sørensen: *Proc. 12th Risø Int. Symp. on Materials Science*, Risø National Laboratory, Roskilde, Denmark, 1991, pp. 489-96.
9. T. Leffers and D. Juul Jensen: *Textures Microstr.*, 1986, vol. 6, pp. 231-63.